Aug 24th, 12:00 AM - Aug 25th, 12:00 AM

Constrained Shape Optimization of Cold-formed Steel Columns

J. Leng

Z. Li

J. K. Guest

B. W. Schafer

Twenty-First International Specialty Conference on Cold-Formed Steel Structures
St. Louis, Missouri, USA, October 24 & 25, 2012

Constrained Shape Optimization of Cold-formed Steel Columns

J. Leng[1], Z. Li[2], J.K. Guest[3] and B.W. Schafer[4]

Abstract

The objective of this paper is to introduce appropriate constraints in the shape optimization of a cold-formed steel column such that the resulting optimized shapes retain the strength benefits of unconstrained optimal solutions combined with practical manufacturing and constructional needs. Unconstrained shape optimization of cold-formed steel columns, where the cross-section that maximizes axial capacity is found, has previously been performed. Here, practical manufacturing and construction constraints are introduced into the optimization algorithm. Members with three lengths: 2 ft, 4 ft, and 16 ft, are considered. Optimized sections from multiple runs show uniformity and bear a close resemblance to unconstrained results. A point-symmetric 'S'-shaped section has maximum capacity for long columns and a singly-symmetric 'Σ'-shaped section with complex lips performs best for shorter columns. The observed strength loss from the unconstrained optimal design, to the constrained optimal design, is within ten percent. A simultaneous perturbation stochastic approximation algorithm, with the idea of injecting randomness in the gradient approximation to save computational cost, is adopted as the local optimizer. A systematic survey on a family of lipped channel cross-sections using the same amount of material was carried out. Comparison reveals that the optimized shapes have much larger capacities and exhibit the potential to seed a new generation of commercial products.

[1] Graduate Research Assistant, Department of Civil Engineering, Johns Hopkins University, Baltimore, MD, USA (jleng1@jhu.edu)
[2] Post-Doctoral Fellow, Department of Civil Engineering, Johns Hopkins University, Baltimore, MD, USA (lizhanjie@jhu.edu)
[3] Assistant Professor, Department of Civil Engineering, Johns Hopkins University, Baltimore, MD, USA (jkguest@jhu.edu)
[4] Professor and Chair, Department of Civil Engineering, Johns Hopkins University, Baltimore, MD, USA (schafer@jhu.edu)

1. Introduction

Cold-formed steel (CFS) members have been extensively used in low and midrise buildings as both load bearing and non-load bearing members due to its high strength-to-weight ratio and low cost of material and manufacture. Typical thickness is about 0.04 in. (1 mm) and the web depth ranges from approximately 3 to 12 in. (75 to 300 mm). A cross-section is fabricated by rolling/bending a given sheet (coil) of steel at a number of discrete positions across the sheet width. Ideally, a given sheet can be bent to nearly any open cross-section. However, currently available North American commercial sections (e.g. AISI cold-formed steel design manual, 2008) are still largely limited to the common C- and Z-sections, leaving a large design space of other shapes still to be explored.

Due to the low thickness and high slenderness of cold-formed steel members, a major design concern is buckling; including local plate buckling, distortional buckling, and global (Euler) buckling (Schafer, 2008). Consequently, an effective way to optimize CFS columns is to maximize the axial capacity of a column with a given length, coil width (i.e., cross-section perimeter), and sheet thickness.

In general, two groups of algorithms have been formulated to tackle this problem. The first type is based on formal mathematical programming, which can find a local minimum but largely relies on the exact or approximate form of partial derivatives of the objective function with respect to design variables, i.e. the gradient or Hessian matrix. On the other hand, a certain number of stochastic search algorithms, like simulated annealing (SA) and genetic algorithms (GA), use injected randomness to search the whole design space in order to find global optima without the requirement on the derivative information. The tradeoff is that the available convergence arguments about these algorithms, if available, are only probabilistic, and multiple runs with a number of function evaluations each time are needed to find a possible optimal design.

The manner in which the objective function is expressed also has a great importance on the formulation of the problem. The classical effective-width method (AISI-S100-07) gets fairly cumbersome for complicated cross-sections. However, the Direct Strength Method (DSM, see Appendix 1 of AISI S100-07), instead, is capable of determining the nominal load P_n for arbitrary geometry columns given the critical load in local (P_{crl}), distortional (P_{crd}), and global buckling (P_{cre}), and the load at yield (P_y). The authors used the finite strip method based on the open source software package CUFSM (Schafer et al., 2006 and 2010) for finding P_{crl}, P_{crd}, and P_{cre}.

The combination of optimization algorithms with code-based strength evaluation criterion has lead to a number of research papers in the CFS optimization field. Lu (2003) combined CUFSM with GA to optimize Z-section dimensions according to the effective width design of Eurocode 3. Kolcu et al. (2010) maximized the critical load P_{cr} computed from Mindlin-Reissner finite strips by using sequential quadratic programming. Recently, Chamberlain Pravia and Kripka (2012) used SA to carry out the dimensional optimization of a C-section column following the effective width method in the AISI specification. Liu et al. (2004) investigated the use of Bayesian classification trees together with DSM and CUFSM in the maximization of P_n. The authors' previous work (Leng et al., 2011) compared the performance of SA, GA and gradient based steepest descent method in unconstrained shape optimization of CFS columns, and developed several novel cross-sections with significant increase in capacity, P_n.

A natural initiative to create more practical cross-sections from optimization makes it necessary to introduce construction and manufacturing constraints into the search process. Constraints in dimensional optimization with the effective width method are normally formulated as inequalities with elementary functions. The constraints developed herein include both shape and dimension constraints, which are not readily expressed explicitly. In this case penalty functions are often employed. However, in the work herein a simple rejection method is employed. If cross-sections violate constraints, as generated from the simulated annealing algorithm, the section is rejected before function evaluation, and a new section is created. Simultaneous perturbation stochastic approximation (SPSA) is adopted as a local optimizer in place of the computational costly steepest decent method with finite difference approximation. Optimization of members with three different physical lengths is performed and the results show only small capacity reductions from the unconstrained optimal shapes. The optimal shapes are also compared with an artificially generated family of lipped channel C-sections using the same coil width and thickness to show the benefit of adopting the optimized sections.

2. Manufacturability constraints in simulated annealing algorithm

As detailed previously (Leng et al., 2011) the selected strategy is to consider the thin sheet of steel comprising a column as being discretized into narrow strips of equal width along the longitudinal direction. At the boundary of these narrow strips the sheet may be bent. Thus, the design vector is formed by the relative turn-angles between strips. Figure 1 (a) illustrates the design variables for a lipped channel C-section. Note, the design vector includes forty-two turn-angles, in the case of the C-section only θ_1, θ_3, θ_9, θ_{35}, and θ_{41} are non-zero. The forty-two turn angles provide an immense freedom to form different shapes.

The C-section of Figure 1 (a) is the initial design for the simulated annealing algorithm; the dimensions are shown in Figure 1 (b). The perimeter of the section is 11 in., t=0.04 in., E=30458 ksi, and F_y=33 ksi. The kernel step of SA is the objective function comparison of a randomly perturbed new design with the current elite design. The geometrically reducing temperature of SA gives rise to the so-called 'hill-climbing' property, allowing SA to accept inferior designs as elite ones more likely at the beginning stage to expand the search space and making it more possible to find a global optimal design ultimately. Details of implementation and theoretical discussion about SA are available in monographs of Arora (2004) and Spall (2003). The improvement presented in this paper from Leng et al. (2011) is the addition of constraints.

The first constraint applied is a symmetry or anti-symmetry condition. A randomly generated tag is used to dictate whether the section will be symmetric. Only half of the forty-two turn-angles is independent, the other half will be determined following the assigned geometric conditions.

The second constraint is the dimension requirement on lips, flanges and the web. In our study, lips and flanges should be no shorter than 0.5 in. and 1.0 in. respectively. This can be done easily using two inequalities for dimensional size optimization, but in shape optimization first the lips and flanges must themselves be identified. The required lengths are divided by element length to calculate the minimum numbers of elements needed for the lip and the flange. Then, two positive integers n_1 and n_2 are generated to make sure the lip and the flange are longer than the minimum values. The nodes on the lip are node 1 to node n_1+1, and node n_1+1 to node n_1+ n_2+1 are on the flange. Note, the algorithm also enforces turn-angles of elements on the flange so that the flange is always flat and parallel with x axis. Finally, symmetry/anti-symmetry condition allows the whole cross-section to be defined. Elements connecting two flanges form the web. The web depth is defined as the distance between two flanges, and must range from 3.625 to 9 in. in this problem.

The third constraint is related to the allowance of the passage of utilities. Usually, the web of a commercial product is punched, leaving spaces for bridging or piping. Thus, there should be enough space between the lips, and any horizontal line in this area cannot intersect with the wall of the cross-section twice to eliminate interference problems. Two terms, the clearance and the back-fold, are helpful to explain the idea. The clearance is defined as the shortest vertical distance between any two points on the two lips. A back-fold is a node on the web which has a smaller vertical coordinate than the previous node. Then, the idea related to this type of constraint is formulated as: the clearance area on the web should be longer than 1.0 in., and there should be no back-folds.

The last constraint is inherited naturally from our previous paper which says the elements of the cross-section cannot overlap in order to make the section feasible. Figure 1 (c) shows a conceived symmetric cross-section as an illustration of the constraints implemented. The procedure of adding these constraints into the new design generation process is given in Figure 2. Finally, our objective function is still directly related to the axial strength of the CFS column determined using DSM, with $\boldsymbol{\Theta}$ denoting the feasible domain of the design vector of turn-angles $\boldsymbol{\theta}$, i.e.

$$P_n = \min\{P_{nl}, P_{nd}, P_{ne}\} \tag{1}$$

$$\min_{\boldsymbol{\theta}\in\boldsymbol{\Theta}}\left(f\left(\boldsymbol{\theta}\right)\right) = \min_{\boldsymbol{\theta}\in\boldsymbol{\Theta}}\left(-P_n\left(\boldsymbol{\theta}\right)\right) \tag{2}$$

where $\boldsymbol{\Theta}$ is determined from the above constraints and is difficult to formulate explicitly.

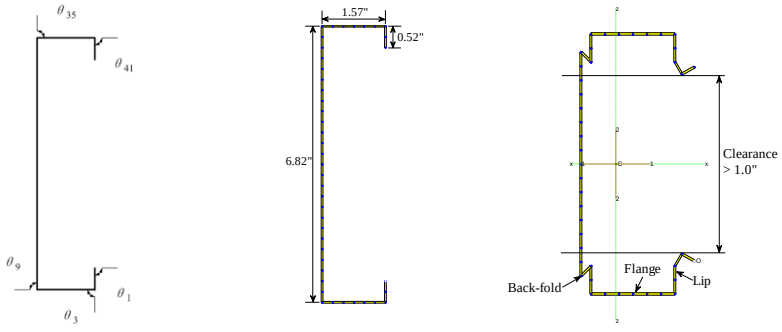

(a) (b) (c)

Figure 1 Illustrations of design variables, initial design and constraints

3. Simultaneous perturbation stochastic approximation algorithm

In our previous work (Leng et al., 2011) finite difference is used to approximate the gradient for the steepest descent method. The major drawback of this approach it is that at least one objective function evaluation is needed to compute one partial derivative. This is fairly costly and hinders use in high dimensional problems. As an alternative, a simultaneous perturbation stochastic approximation (SPSA) algorithm is used. SPSA only uses two function evaluations to approximate the gradient vector. Like steepest descent, SPSA updates the design vector iteratively using a form of the 'gradient', $\boldsymbol{g}_k(\boldsymbol{\theta}_k)$.

$$\boldsymbol{\theta}_{k+1} = \boldsymbol{\theta}_k - a_k \boldsymbol{g}_k\left(\boldsymbol{\theta}_k\right) \tag{3}$$

$$\boldsymbol{g}_k\left(\boldsymbol{\theta}_k\right) = \begin{bmatrix} \dfrac{f\left(\boldsymbol{\theta}_k + c_k\Delta_k\right) - f\left(\boldsymbol{\theta}_k - c_k\Delta_k\right)}{2c_k\Delta_{k1}} \\ \vdots \\ \dfrac{f\left(\boldsymbol{\theta}_k + c_k\Delta_k\right) - f\left(\boldsymbol{\theta}_k - c_k\Delta_k\right)}{2c_k\Delta_{kp}} \end{bmatrix} \tag{4}$$

$$= \frac{f\left(\boldsymbol{\theta}_k + c_k\Delta_k\right) - f\left(\boldsymbol{\theta}_k - c_k\Delta_k\right)}{2c_k}\left[\Delta_{k1}^{-1}, \Delta_{k2}^{-1}, \cdots, \Delta_{kp}^{-1}\right]^T$$

Note that (4) has a form that resembles the central difference method, but the inherent distinction is that the p-dimensional perturbation vector of this algorithm, $\Delta_{ki} = [\Delta_{k1}, \Delta_{k2}, \cdots, \Delta_{kp}]^T$, is random and has zero mean. A Bernoulli ±1 distribution is used to generate Δ_{ki}, which has the same probability to be positive or negative one. The sequence $\{a_k\}$ serves as step-lengths, and $\{c_k\}$ contains magnitudes of the perturbation in the partial derivative calculation. According to Spall (2003), it is advised to use decaying sequences of $\{a_k, c_k\}$ taking the following forms

$$a_k = \frac{a}{(k+1+A)^{\alpha}} \text{ and } c_k = \frac{c}{(k+1)^{\gamma}} \tag{5}$$

where a, A, α, c, and γ are positive parameters to be tuned. In this work $\alpha = 1$, $\gamma = 1/6$, $A = 50$, $a = 0.5$, and $c = 0.1$ was used.

4. Column optimization result

To incorporate the possible impact of the controlling buckling mode (i.e., local, distortional, or global) on the optimization results, columns with three distinct physical lengths: 2, 4 and 16 ft were investigated. The major change in the simulated annealing parameters is the increase of the maximum number of cooling iterations m_{max}, which is 25, 35, and 100 for 2, 4, and 16 ft columns, respectively. This implies that the algorithm is allowed a greater number of iterations when searching for a global optimum in the longer columns. All other SA parameters remain the same. The number of trial designs within one temperature iteration is $k_{max} = 200$, and the temperature cooling rate is $r = 0.5$. The computation cost for the constrained optimization is significantly higher than the previously conducted unconstrained optimization.

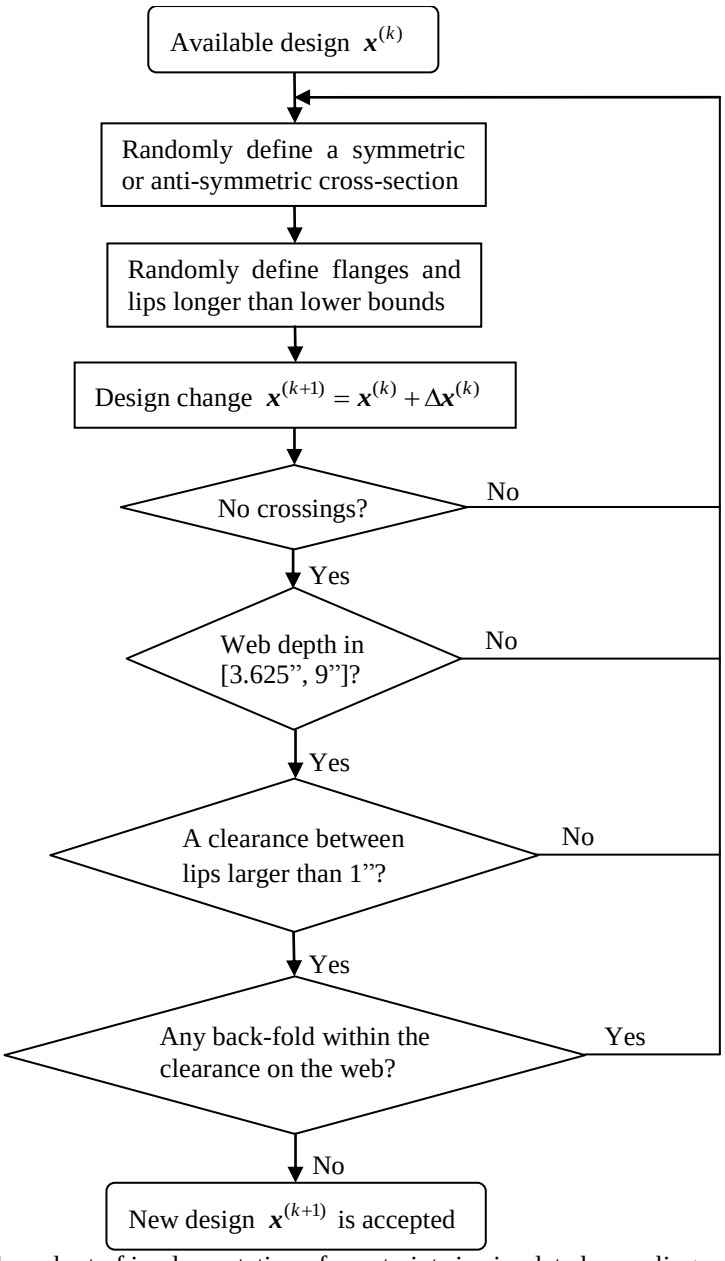

Figure 2 Flow chart of implementation of constraints in simulated annealing

4.1. Short length (2 ft) column

Starting from the C-section of Figure 1 (b), SA optimization is run ten times for 2 ft long columns. The best two results are depicted in Figure 3. Both sections are symmetric, have relatively long complex lips at the free ends, and corrugations in the web. The results are similar to what is commonly referred to as a sigma, i.e., Σ-section. Since these members are fairly short, the role played by global buckling is trivial. Corrugations in the web reduce the unstiffened plate width greatly and provide significant resistance to local buckling. As discussed by Schafer et al. (2006), complex stiffeners are able to provide improved ultimate strength performance over simple stiffeners. For local buckling, they have shown inward angled stiffeners can: '(1) sustain higher buckling loads, as the stiffener provides positive rotational restraint to the attached plate, and (2) demonstrate less sensitivity over a wide range of plate (flange) widths'. The inward angled stiffener also renders an efficient solution for elastic distortional buckling by moving the shear center of the stiffener/flange assembly away from the flange/lip juncture and further away from the flange/web juncture.

Numerical comparison is given in Table 1 below. Critical buckling loads and nominal strengths of the three modes of the C-section in Figure 1 (b) and the sections in Figure 3 are all listed. It may be observed that the optimized shape increases P_n by 126% from the original C-section. This extent of increased capacity is roughly the same of that arrived at in previous unconstrained optimization. This not only shows the desirable performance of the optimized designs, but also demonstrates the usefulness of SA with constraints. The data also reveals that the optimized shapes have P_{nd} = 14.32 kips which equals the squash load P_y, implying that distortional buckling is not detrimental for these shapes. Figure 4 is the convergence curve of the cross-section in Figure 3 (a). The fluctuation of P_n at the beginning suggest acceptance of some inferior designs as the elite one, while the final optimal strength P_n is 95.5% of P_y.

(a) P_n = 13.68 kips (b) P_n = 13.66 kips

Figure 3 Optimal cross-sections found by SA for 2 ft column

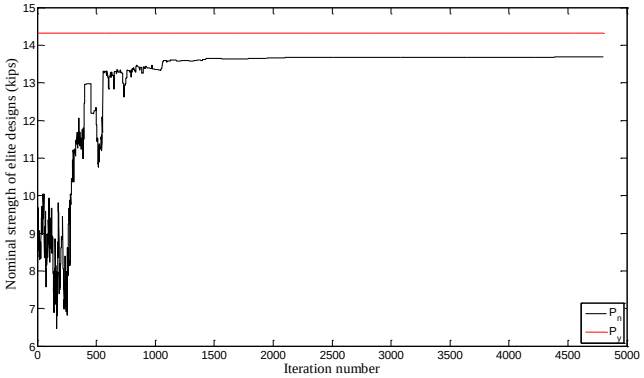

Figure 4 Convergence curve of P_{nelite} for cross-section in Figure 3 (a)

4.2. Intermediate length (4 ft) column

The same analysis procedure is repeated for 4 ft long columns. The two best cross-sections in Figure 5 resemble the optimal Σ-shapes from the 2 ft columns. The distance between the two ends of the section in Figure 5 (b) is close to 1.0 in., suggesting the algorithm searches at the boundaries of the constraints even with the rather heuristic approach adopted in the constraint enforcement. The values in Table 1 indicate that the controlling mode is also the same as the 2 ft columns. An increased capacity of 135% from the C-section is achieved.

In comparison with previous work (Leng et al., 2011), the constrained optimal shapes are competitive, representing only a 3.8% strength drop from the 'Bobby pin' sections previously identified. However, these shapes are much more practical than the irregular looking unconstrained optima.

(a) P_n = 12.25 kips (b) P_n = 12.20 kips

Figure 5 Optimal cross-sections found by SA for 4 ft column

Table 1 Critical and nominal loads of C- and "Σ"–sections

Member length (ft.)	Figure	P_{crl} (kips)	P_{crd} (kips)	P_{cre} (kips)	P_{nl} (kips)	P_{nd} (kips)	P_{ne} (kips)	P_n (kips)
2	1b	2.32	5.12	68.64	6.07	6.69	13.12	6.07
2	3a	38.77	45.27	131.45	13.68	14.32	13.68	13.68
2	3b	52.67	39.22	127.17	13.66	14.22	13.66	13.66
4	1b	2.32	5.12	18.36	5.22	6.69	10.33	5.22
4	5a	43.19	49.61	38.33	12.25	14.32	12.25	12.25
4	5b	54.01	26.22	37.29	12.20	13.19	12.20	12.20

4.3. Long length (16 ft) column

SA runs of the 16 ft columns yield different optimal shapes from the short and intermediate length columns due to global buckling. Eight of the ten final SA optimized shapes are anti-symmetric. However, the squashed 'S' cross-sections in Figure 6 closely match unconstrained optima (Leng et al., 2011), incurring only a 7.2 percent drop of strength due to the constraints. Note, these S-sections bear 187% more strength than the 16 ft long C-seciton of Figure 1 (b). The cross-section properties are compared in Table 2 and the features associated with flexural-torsional buckling of the squashed 'S' sections in the previous unconstrained optimization work is also provided.

The optimal global section includes a number of key features. First, the final sections are point-symmetric so the shear center and centroid coincide naturally. Second, constrained optimization fails to make the principal moments of inertia I_{11} and I_{22} equal, as was advantageously accomplished in the unconstrained optimization. The significance of this is real - even with higher I_{11} and warping coefficient C_w, the constrained optimization section of Figure 6 (b) still performs a bit worse than the previous unconstrained optimization. Finally, the optimal sections in Figure 6 both have lips of only two elements, indicating the minimum value allowed by lip length constraints is active in this case.

(a) P_n = 2.96 kips (b) P_n = 2.90 kips

Figure 6 Optimal cross-sections found by SA for 16 ft column

Table 2 Cross-section properties of squashed 'S' sections of 16 ft. member

Section	Figure	I_{11} (in^4)	I_{22} (in^4)	C_w (in^6)	$\sqrt{x_0^2 + y_0^2}$ (in)	P_n (kips)
squashed 'S'	6a	0.842	0.414	2.408	0	2.96
squashed 'S'	6b	0.898	0.406	2.440	0	2.90

4.4. Further refinement using SPSA

To refine the stochastic search (SA) optimal sections SPSA is utilized on the 4 ft long columns. One thousand function evaluations are budgeted. According to Spall (2003), the parameter A in (5) is set as $A = 0.1 \times 1000 / 2 = 50$. The flange elements (parallel to x axis) are fixed and not updated, and no other constraints above are introduced into SPSA. Since we use SPSA for local optimization, the step-length in each iteration is small. Thus, a gain sequence $\{a_k, c_k\}$ with $\alpha = 1$, and $\gamma = 1/6$ is chosen. After trial-and-error, a and c are set to 0.5 and 0.1 respectively.

Several trials are completed. The best two in terms of terminal P_n are presented in Figure 7. The common feature is that the stochastic approximated gradient tries to form a hump in the middle of the web and drive the lips together. As a result, the web and lips are smoothed, but both shapes violate the clearance length constraint. With the approximate gradient and predefined gain sequence, P_n is not guaranteed to increase in every iteration. Still, the terminal design can grow, here an increase of 0.4% over the SA optimal shape is realized.

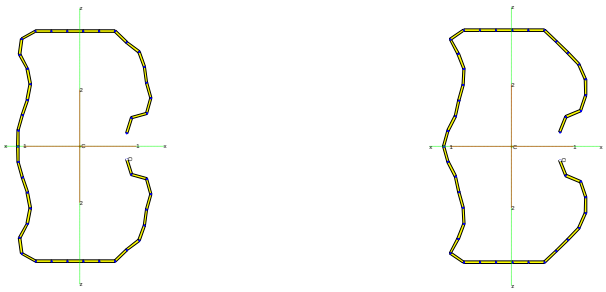

(a) P_n = 12.30 kips (b) P_n = 12.27 kips

Figure 7 SPSA refined cross-sections of Figure 5 (a)

5. Performance comparison with a C-section family

The optimized members reported herein use a particular amount of material. The total perimeter width is 11 in. and the thickness is 0.04 in. Although the developed sections are shown to beat the initial C-section of Figure 1 (b) how much better is the optimal sections than the optimal C-section? To answer this question and show the potential for a new family of optimal shapes, the optimal shapes developed here are compared to all practical C-sections that could be created from the fixed initial amount of material.

The full set of potential C-sections with a perimeter width of 11 in., t=0.04 in., E=30458 ksi, and F_y=33 ksi are created. The web height h is varied from 0.5 to 10 inches, flange width b from 0.5 to 5 inches, and the lips d vary within the permissible formulation (total perimeter width = 11 in.) for the C-section. The resulting C-section is modeled as straight-line model with the recommended procedures given by Li and Schafer (2010). Strength is determined by DSM.

The axial and bending capacities of the C-sections are normalized by cross-sectional area and plotted in Figure 8. In addition, the optimal sections at 2 ft, 4 ft, and 16 ft are similarly normalized and included. Optimal beam cross-sections, following the same algorithm to that reported here for columns, have also been generated. These optimal sections are also added to Figure 8 for comparison.

Figure 8 demonstrates the efficiency of the optimization algorithm. The optimized sections handily beat any possible C-section member while using the same amount of material. The optimal sections are better than the C-section for any combination of axial or bending moment. Optimal sections have the potential to increase the efficiency and applicability of CFS members. Further, aligned with LEED (2007) minimizing material may enhance the sustainability of the final building. Inspired by the performance of these optimized cross-sections, a family of new CFS member shapes is being developed using formal optimization tools in the context of a U.S. National Science Foundation cooperative research grant between the authors and an Egyptian research team.

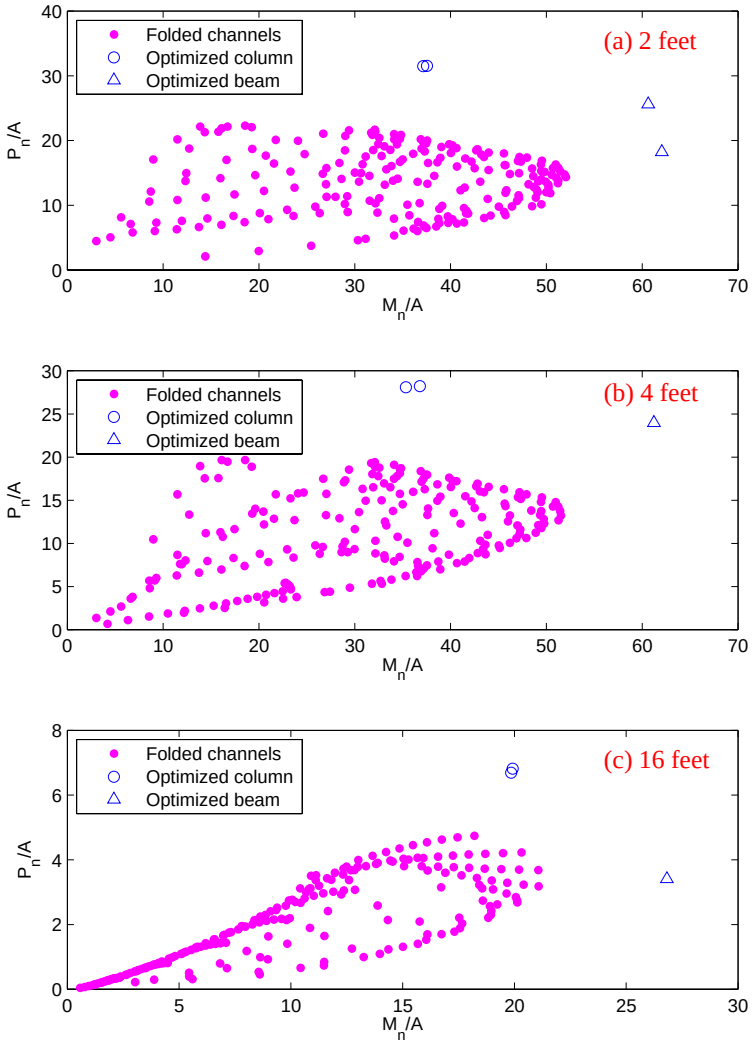

Figure 8 Material efficiency of folded channels and optimized shapes

6. Conclusions

Free-form shape optimization of cold-formed steel members utilizing a simulated annealing algorithm for the optimization and objective function evaluation driven by the finite strip method for stability analysis and the Direct

Strength Method for strength prediction is shown to produce optimal shapes with over 130% increase in axial strength compared with conventional C-sections. Further, it is shown that practical constructional and manufacturing constraints: singly- or point-symmetric sections, parallel and flat flanges of minimum width, minimum web clear width for creating holes for services, minimum end lip length, etc., may all be successfully introduced into the optimization method. The resulting constrained optimization has only a modest decrease in capacity compared with unconstrained optimization and leads to practical optimal shapes: the singly-symmetric Σ-section for short and intermediate columns, and the point-symmetric S-section for long unbraced columns. Comparison of the optimal shapes to the full family of conventional lipped channel C-sections with the same amount of material shows that the developed optimal shapes have increased capacity for a complete range of axial load and major-axis bending. Inspired by these results the authors are working on developing a complete family of optimal shapes for cold-formed steel.

Acknowledgments

This project received partial funding from U.S. National Science Foundation project: NSF-OISE-1103894: US Egypt Cooperative Research: Use of Cold-Formed Steel in Residential Housing. Any opinions, findings, and conclusions or recommendations expressed in this publication are those of the author(s) and do not necessarily reflect the views of the National Science Foundation.

References

American Iron and Steel Institute. (2007). North American specification for the design of cold-formed steel structural members (AISI S100-2007 ed.). Washington DC: American Iron and Steel Institute.

American Iron and Steel Institute. (2008). Cold-formed steel design manual (D100-08 ed.). Washington DC: American Iron and Steel Institute.

Arora, J. S. (2004). Introduction to optimum design (2nd ed.) Academic Press.

Chamberlain Pravia, Z. M., & Kripka, M. (2012). Cross section optimization using simulated annealing of cold-formed steel channel columns. Proceedings of the Annual Stability Conference Structural Stability Research Council, Grapevine, TX.

Kolcu, F., Ekmekyapar, T., & Özakça, M. (2010). Linear buckling optimization and post-buckling behavior of optimized cold formed steel members. Scientific Research and Essays, 5(14), 1916-1924.

Leng, J., Guest, J. K., & Schafer, B. W. (2011). Shape optimization of cold-formed steel columns. Thin-Walled Structures, 49(12), 1492-1503.

Li, Z., & Schafer, B. W. (2010). Application of the finite strip method in cold-formed steel member design. Journal of Constructional Steel Research, 66(8), 971-980.

Liu, H., Igusa, T., & Schafer, B. (2004). Knowledge-based global optimization of cold-formed steel columns. Thin-Walled Structures, 42(6), 785-801.

Lu, W. (2003). Optimum design of cold-formed steel purlins using genetic algorithms Helsinki University of Technology.

Schafer, B. W. (2008). Review: The direct strength method of cold-formed steel member design. Journal of Constructional Steel Research, 64(7), 766-778.

Schafer, B. W. (2010). User's manual and tutorials of CUFSM 3.12 Johns Hopkins University. http://www.ce.jhu.edu/bschafer/cufsm/cufsm312/index.htm

Schafer, B. W., & Ádány, S. (2006). Buckling analysis of cold-formed steel members using CUFSM: Conventional and constrained finite strip methods. Eighteenth International Specialty Conference on Cold-Formed Steel Structures, pp. 39-54.

Schafer, B. W., Sarawit, A., & Peköz, T. (2006). Complex edge stiffeners for thin-walled members. Journal of Structural Engineering, 132(2), 212-226.

Spall, J. C. (2003). Introduction to stochastic search and optimization: Estimation, simulation, and control. Hoboken, NJ: John Wiley and Sons.

Steel Stud Manufacturers Association. (2011). Product technical information complies with 2009 IBC SSMA. http://www.ssma.com

U.S. Green Building Council. (2007). LEED-NC version 2.2 reference guide. Washington, DC: USGBC.